

Paleoceanography and Paleoclimatology










RESEARCH ARTICLE

10.1029/2022PA004493

Transient Shoaling, Over-Deepening and Settling of the Calcite Compensation Depth at the Eocene-Oligocene Transition

Key Points:

- A short-lived calcite compensation depth (CCD) shoaling event occurred in the latest Eocene associated with a negative excursion in oceanic $\delta^{13}\text{C}$
- The two-step Eocene-Oligocene Transition CCD deepening occurred in both the Pacific and Atlantic Oceans
- First CCD deepening step is coupled to recovery from latest Eocene shoaling event and the second CCD step is coupled to Antarctic glaciation

V. E. Taylor^{1,2} , T. Westerhold³ , S. M. Bohaty^{1,4} , J. Backman⁵, T. Dunkley Jones⁶ , K. M. Edgar^{1,7} , K. E. Egan^{1,8}, M. Lyle⁹, H. Pälike², U. Röhl² , J. Zachos¹⁰, and P. A. Wilson¹ 

¹School of Ocean and Earth Science, Waterfront Campus, National Oceanography Centre, University of Southampton, Southampton, UK, ²Now at Department of Earth Sciences, University of Bergen, and Bjerknes Centre for Climate Research, Bergen, Norway, ³MARUM – Center for Marine Environmental Sciences, University of Bremen, Bremen, Germany, ⁴Now at Institute of Earth Sciences, Heidelberg University, Heidelberg, Germany, ⁵Department of Geological Sciences, Stockholm University, Stockholm, Sweden, ⁶School of Geography, Earth and Environmental Sciences, University of Birmingham, Birmingham, UK, ⁷Now at School of Geography, Earth and Environmental Sciences, University of Birmingham, Birmingham, UK, ⁸Now at Flood Forecasting Centre, Met Office, Exeter, UK, ⁹College of Earth, Ocean and Atmospheric Science, Oregon State University, Corvallis, OR, USA, ¹⁰Department of Earth and Planetary Sciences, University of California, Santa Cruz, CA, USA

Supporting Information:

Supporting Information may be found in the online version of this article.

Correspondence to:

V. E. Taylor,
victoria.taylor@uib.no

Citation:

Taylor, V. E., Westerhold, T., Bohaty, S. M., Backman, J., Dunkley Jones, T., Edgar, K. M., et al. (2023). Transient shoaling, over-deepening and settling of the calcite compensation depth at the Eocene-Oligocene Transition. *Paleoceanography and Paleoclimatology*, 38, e2022PA004493. <https://doi.org/10.1029/2022PA004493>

Received 14 JUN 2022
Accepted 8 MAY 2023

Abstract The major Cenozoic shift from a shallow (~3–4 km) to deep (~4.5 km) calcite compensation depth (CCD) occurred at the Eocene-Oligocene Transition (~34 Ma), suggesting a strong relationship between calcium carbonate (CaCO_3) cycling and Antarctic glaciation. However, the linkages between these two events are debated. Here we present new records of bulk sediment stable isotope and carbonate composition from a depth transect of sites in the low-latitude Pacific Ocean and one site from the South Atlantic Ocean, together with a new benthic foraminiferal stable isotope record ($\delta^{13}\text{C}_b$ and $\delta^{18}\text{O}_b$) from the Pacific where the sedimentary sequence is most expanded. Our records reveal a short-lived (~3,000 Kyr) CCD shoaling event closely associated with a negative carbon isotope excursion in the latest Eocene. This event is immediately followed by CCD deepening which occurs in two rapid (~40 Kyr-long) steps. Our data show that the first of these deepening steps represents recovery from the latest Eocene shoaling event while the second was closely associated with a rapid increase in $\delta^{18}\text{O}_b$ and shows a distinctive over-deepening and settling pattern to >5 and 4.4 km, respectively. These results, together with good agreement between Pacific and South Atlantic records, strongly suggest that the carbon cycle was perturbed globally shortly before the inception of Antarctic glaciation. Once large-scale Antarctic glaciation was initiated, rapid further change in global seawater chemistry triggered transitory deep ocean carbonate burial fluxes far exceeding their early Oligocene steady state values.

1. Introduction

Biogenic calcium carbonate (CaCO_3) is formed widely in the upper open ocean, and incorporated into the shells and liths of living marine plankton, but post-mortem settling through the water column leads to its dissolution at depth so that CaCO_3 eventually disappears from marine sediments at some level marking the calcite compensation depth (CCD). The CCD is controlled by the balance between carbonate input to the oceans down rivers and output through burial in marine sediments. On geological timescales, these fluxes are controlled by volcanic and metamorphic outgassing and continental weathering, which in turn govern atmospheric carbon dioxide concentrations (Broecker & Peng, 1987; Dutkiewicz et al., 2018; Müller et al., 2022; Ridgwell & Zeebe, 2005; van Andel et al., 1975). Records of CCD change in the equatorial Pacific Ocean document two distinct CCD regimes for the Cenozoic era: a shallow (~3.5 km) regime with pronounced transient fluctuations during the early Cenozoic and a deeper (~4.5 km) more stable regime during the later Cenozoic (Lyle et al., 2005, 2019; Pälike et al., 2012; van Andel, 1975). The shift between these two regimes occurs at the Eocene-Oligocene Transition (EOT; ~34 Ma) when the CCD in the equatorial Pacific Ocean deepened by ~1 km (Coxall et al., 2005; Pälike et al., 2012; Rea & Lyle, 2005). Detailed records for the EOT from one site in the deep equatorial Pacific (Ocean Drilling Program [ODP], Site 1218) are characterized by two abrupt, near-synchronous increases in both CaCO_3 content and benthic foraminiferal $\delta^{18}\text{O}$ and $\delta^{13}\text{C}$ ($\delta^{18}\text{O}_b$ and $\delta^{13}\text{C}_b$, respectively), suggesting intimate coupling between the carbon cycle, accelerated cooling of the high latitudes, and the inception of sustained large-scale glaciation of Antarctica (Coxall et al., 2005).

© 2023. The Authors.

This is an open access article under the terms of the [Creative Commons Attribution License](https://creativecommons.org/licenses/by/4.0/), which permits use, distribution and reproduction in any medium, provided the original work is properly cited.

To explain the apparent teleconnection between Antarctic glaciation and carbonate chemistry in the deep equatorial Pacific Ocean, Coxall et al. (2005) favored a shift in the locus of global carbonate burial away from the shelves to the ocean basins in response to glacioeustatic sea level fall, that is, “shelf–basin fractionation” (Berger & Winterer, 1975; Opdyke & Wilkinson, 1988). Armstrong McKay et al. (2016) and Merico et al. (2008) tested this suggestion against competing hypotheses using biogeochemical box models with nutrient cycling capability and found that, of all the hypotheses tested, shelf–basin fractionation provided the best match to the available data. In this shelf–basin fractionation explanation, CCD deepening is driven by (a) a temporary spike in carbonate weathering from newly exposed shelf limestones and (b) a sustained increase in carbonate burial in the basins attributable to decreased shelf area and thus decreased carbonate burial on the shelves. Yet, shelf–basin fractionation has been called into question for two principal reasons. First, the initial increase in $\delta^{18}\text{O}_b$ of the EOT is interpreted to be primarily driven by cooling rather than Antarctic glaciation (Lear et al., 2008; Miller et al., 2008). Second, the EOT CCD deepening is suggested to be too large to be explained solely by shelf–basin fractionation (Rea & Lyle, 2005). Many other mechanisms have, therefore, been considered to help explain the link between carbon cycling, CCD deepening, and climate change at the EOT. Some of these mechanisms (e.g., increased input of Ca to the oceans; drawdown of CO_2 from the atmosphere and input of alkalinity to the ocean through increased silicate weathering; increased organic carbon burial in marine sediments) are untenable based on the box model results (Merico et al., 2008), while two others (increased net sequestration of carbon into ^{12}C -rich capacitors such as terrestrial peat deposits, and increased ocean ventilation), when combined with shelf-basin fractionation, are more plausible (Armstrong McKay et al., 2016).

Despite these model-based advances in understanding EOT deep-sea records, a major obstacle to further progress is our continued reliance on data from a single site (ODP Leg 199 Site 1218) to assess the detailed relationship between CaCO_3 burial and climate at the EOT. This weakness is exacerbated by the occurrence of a stratigraphically condensed interval of non- CaCO_3 deposition immediately prior to CCD deepening in the latest Eocene at Site 1218 that prevents a close examination of the initiation of EOT climate and CCD changes. Records from different water depths and ocean basins are therefore needed. Here we present new detailed records of bulk sediment stable isotopes and carbonate content from a depth-transect of sites in the low-latitude Pacific Ocean, which allow us to determine the magnitude and sequence of CCD changes across the EOT and a new benthic stable isotope stratigraphy from the shallowest of these sites where the sequence is most expanded. We also present a carbonate content record from subantarctic South Atlantic ODP Leg 177 Site 1090 to test whether the carbonate burial history documented in the equatorial Pacific is a regional feature or more globally representative.

1.1. EOT Chemostratigraphy

Based on previous analysis of ODP Leg 199 cores, the benthic foraminiferal stable isotope record from Site 1218 ($8^\circ 53.378'\text{N}$, $135^\circ 22.00'\text{W}$; $\sim 3,750$ m paleodepth; Figure 1) has provided a benchmark chemostratigraphy for the EOT. That record is defined by two rapid (≤ 40 Kyr estimated duration) pronounced $\delta^{18}\text{O}_b$ and $\delta^{13}\text{C}_b$ “steps” to higher values, both closely associated with abrupt increases in the CaCO_3 content of sediments at Site 1218 (Coxall et al., 2005; Coxall & Wilson, 2011). At Site 1218, the first of these $\delta^{18}\text{O}_b$ increases, Step 1, has an amplitude of $\sim 0.6\text{‰}$, but its duration is poorly constrained because of a stratigraphically condensed interval of non- CaCO_3 deposition in the latest Eocene at this site (Coxall et al., 2005; Coxall & Wilson, 2011). Temperature reconstructions from sites situated elsewhere and in shallower water suggest this initial $\delta^{18}\text{O}_b$ increase is largely driven by cooling of the surface and deep ocean, with a minor increase in continental ice volume (Katz et al., 2008; Lear et al., 2004, 2008, 2010; Pusz et al., 2011; Wade et al., 2012). The second step increase in $\delta^{18}\text{O}_b$, Step 2, is larger (at least 0.9‰) and occurs during the earliest Oligocene (Coxall et al., 2005; Coxall & Wilson, 2011). These two step-increases in the $\delta^{18}\text{O}_b$ record are separated by an intervening ~ 300 Kyr-long “plateau” interval of minimal change. The Site 1218 $\delta^{18}\text{O}_b$ record resembles the output from coupled climate–ice sheet model experiments in which Antarctic glaciation is triggered by a threshold response to slowly declining atmospheric carbon dioxide levels (DeConto & Pollard, 2003). Analysis of Southern Ocean drill cores indicates an abrupt appearance of ice-rafted debris (IRD) and chemically immature clay minerals (Ehrmann & Mackensen, 1992; Hambrey et al., 1991; Zachos et al., 1992) correlative with Step 2 (Scher et al., 2011) (earliest Oligocene oxygen isotope step [EOIS], in the terminology of Hutchinson et al., 2021), suggesting this rapid $\delta^{18}\text{O}_b$ increase marks the onset of sustained large-scale Antarctic glaciation. The early Oligocene glacial maximum (EOGM, ~ 33.65 to ~ 33.16 Ma; after Liu et al., 2004) immediately follows Step 2 (EOIS) and is interpreted to represent a near 500 Kyr-long interval of peak glacial conditions (Liu et al., 2004).

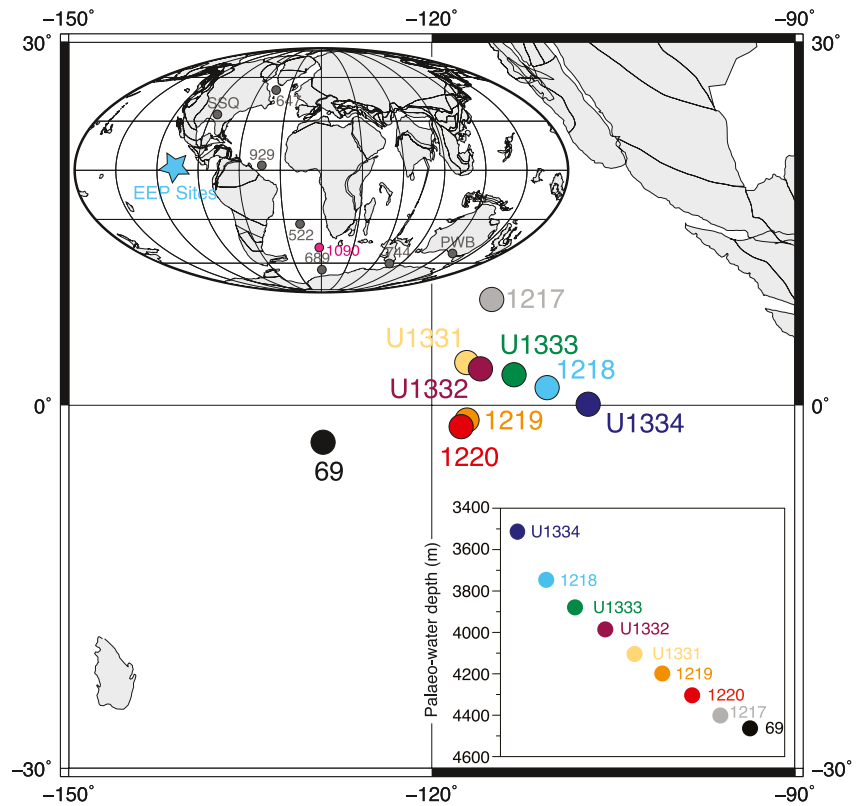


Figure 1. Location of sites studied. Main panel shows sites from the eastern equatorial Pacific Ocean (EEP) including those used for our palaeowater depth transect (see inset bottom right). Inset (top left) shows site studied in the South Atlantic Ocean (ODP 1090) together with other sites referred to in the text. Sites are shown in their palaeo-locations at 34 Ma and span a palaeo-water depth of ~3,500 to 4,500 m (inset). (SSQ, St. Stephen's Quarry; PWB, Port Willunga Beach). Inset map (paleogeographic reconstruction for 34 Ma) generated using <http://www.odsn.de>. Palaeo-locations of sites in the eastern equatorial Pacific taken from Pälিকে et al. (2012) and calculated using Koppers et al. (2001). Palaeo-water depth estimates at 34 Ma for sites in the eastern equatorial Pacific taken from Pälিকে et al. (2012).

While the benthic foraminiferal stable isotope record from Site 1218 is well defined for the earliest Oligocene (Coxall et al., 2005; Coxall & Wilson, 2011), low CaCO_3 contents, slow sedimentation rates and variable benthic foraminiferal assemblages and preservation in sediments of latest Eocene age make this part of the record more challenging to interpret. These issues are most acute at the base of the EOT where an extremely condensed interval of non-carbonate burial occurs limiting information on the sequence of events leading up to the initiation of large-scale sustained Antarctic glaciation. Low sedimentation rates and temporal resolution are also a feature in the record from St. Stephen's Quarry, (Gulf Coast USA) where at least three $\delta^{18}\text{O}$ increases, including a “failed” late Eocene glaciation event, are inferred (Katz et al., 2008).

2. Materials and Methods

2.1. Study Sites

Integrated Ocean Drilling Program (IODP) Expedition 320, the “Pacific Equatorial Age Transect” (PEAT), recovered continuous sedimentary sequences from a depth transect of sites in the eastern equatorial Pacific (EEP) (Figure 1). New sedimentary sections spanning the EOT were recovered at four sites (IODP Sites U1331–U1334). Together with sections from ODP Leg 199 (ODP Sites 1217–1220), these archives form a palaeo-water depth transect spanning ~3,500 to 4,500 m in the EEP (Pälিকে et al., 2012) (Figure 1, inset). Site U1334 was strategically positioned to target the EOT from a shallower palaeo-water depth than Site 1218 to recover a more carbonate-rich and expanded late Eocene sequence. For all sites we use the revised composite depth scales (m, rmcd) of Westerhold et al. (2012). Decimeter-scale site-to-site correlations in the depth domain were achieved using physical properties and x-ray fluorescence (XRF) core scanning datasets, constrained by magnetostratigraphic

reversal positions and biostratigraphic datum levels (Westerhold et al., 2012, 2014). A common stratigraphy for the PEAT sites was achieved by transferring the astronomically calibrated age model for Sites U1334, 1218, and U1333, based on the tuning of calibrated Si, Fe, and Ca XRF core scanning data to the stable long (405-kyr) eccentricity cycle (Westerhold et al., 2014), to Sites 1217, 1219, 1220, U1331 and U1332. The tuning strategy did not use stable isotope records (Westerhold et al., 2012, 2014), and so these correlations can now be independently assessed using our bulk sediment stable isotope records (see below). Bulk sediment $^{187}\text{Os}/^{188}\text{Os}$ records are also available for Sites 1218 and 1219 (Dalai et al., 2006) and provide an additional useful independent check on correlations between the shallow sites and deeper more condensed ones where CaCO_3 is absent in the uppermost Eocene (Figure S1 in Supporting Information S1).

South Atlantic ODP Leg 177 Site 1090 (42°58.8'S, 8°53.9'E) is located on the southern flank of the Agulhas Ridge (Figure 1) with a present-day water depth of ~3,700 m (Gersonde et al., 1999) and an estimated palaeo-water depth of ~3,000–3,300 m at 34 Ma (Pusz et al., 2011). We updated the Site 1090 magnetostratigraphic age model (Channell et al., 2003) using magnetochron boundary ages calculated from the astronomically tuned age model of equatorial Pacific Sites U1334, 1218, and U1333 (Westerhold et al., 2014). We also reinterpreted the normal polarity interval identified as “Subchron C13r.1n” (Channell et al., 2003) as C15n, which yields a sedimentation rate history consistent with the high biogenic silica contents in lowermost C13r. We then correlated Site 1090 to the sites in the equatorial Pacific using the benthic foraminiferal $\delta^{13}\text{C}$ records from Site U1334 (this study) and Site 1090 (Pusz et al., 2011).

2.2. Benthic Foraminiferal Stable Isotopes

To construct the benthic foraminiferal stable isotope stratigraphy for Site U1334 (present day: 7°59.998'N, 131°58.408'W; ~3,500 m paleodepth at 34 Ma; Figure 1), approximately 20 cc samples were taken at 2-cm to 4-cm intervals between 286.94 and 304.75 m rmd following the revised composite splice of Westerhold et al. (2012). The samples were oven-dried at 50°C, soaked in a 0.2% sodium hexametaphosphate solution until disaggregated, washed over 63 μm sieves with deionized (DI) water, and then oven-dried overnight at 50°C. Sample weights were recorded before and after all sample processing steps. Coarse fraction residues were dry sieved and *Cibicides grimsdalei* specimens were picked from the 250–355 μm sieve fraction. Benthic foraminifera of Eocene and Oligocene age at Site U1334 appear to robustly record primary isotopic signals (Edgar et al., 2013). The best preserved 5–10 specimens picked from each sample were gently broken open between glass slides, ultrasonically cleaned in pure methanol, and rinsed in DI water to remove adhering clays and calcareous infilling. The cleaned foraminiferal fragments were oven dried at 50°C and 30–70 μg sub-samples were weighed into reaction vials. Analyses were conducted in the Stable Isotope Ratio Mass Spectrometry Laboratory at the University of Southampton's Waterfront Campus, National Oceanography Centre (NOCS) using a Thermo Scientific Kiel IV Carbonate Device coupled to a Thermo Scientific MAT-253 isotope ratio mass spectrometer. Isotope ratios were calibrated to the Vienna Pee Dee Belemnite (VPDB) scale through a two-point calibration using NBS-19 and NBS-18. Repeat analysis of an in-house consistency standard (GS1) measured alongside samples indicates an inter-run analytical precision that is better than 0.03 and 0.08‰ for $\delta^{13}\text{C}$ and $\delta^{18}\text{O}$, respectively.

2.3. Bulk Sediment Stable Isotope Series

To independently verify the site-to-site correlations of Westerhold et al. (2012, 2014), bulk sediment stable isotope data were generated for Sites U1331–U1334, 1217, and 1219–1220. For these analyses, small (~0.5 g) samples of bulk sediment were taken at 1- to 5-cm intervals, oven-dried at 50°C, and ground into a fine homogenized powder using an agate pestle and mortar. The data for Sites U1331, U1334, 1217, and 1220 were generated in the Stable Isotope Ratio Mass Spectrometry Laboratory at the University of Southampton's Waterfront Campus, NOCS. These analyses were conducted using a Europa GEO 20-20 mass spectrometer equipped with an automated carbonate preparation system. The data for Site U1332 were generated at the University of California Santa Cruz (UCSC) using a Kiel Carbonate Device coupled to a MAT-253 isotope ratio mass spectrometer. At both laboratories, external analytical precision, based on repeated analysis of in-house standards calibrated to NBS-19, is better than 0.1‰ for both $\delta^{13}\text{C}$ and $\delta^{18}\text{O}$. Site U1333 bulk sediment stable isotope data were produced at MARUM, University of Bremen, following the approach detailed in Westerhold et al. (2014). Data for Site 1219 were generated at Stockholm University using a Kiel II Carbonate Device coupled to a Finnegan MAT-252 mass spectrometer. Repeated measurements of NBS-19 alongside samples returns a standard deviation of 0.04

and 0.10‰ for $\delta^{13}\text{C}$ and $\delta^{18}\text{O}$, respectively. Bulk sediment stable isotope data for Site 1218 are from Coxall et al. (2005). All results are reported relative to VPDB.

2.4. Carbonate Content and Accumulation

To generate records of carbonate content and accumulation across the equatorial Pacific depth transect, discrete bulk sediment samples (~0.5 g) were taken at 1- to 5-cm intervals from Sites U1331–U1334, 1217, and 1219–1220, oven-dried at 50°C, and ground into a fine homogenized powder using an agate pestle and mortar. High precision wt% CaCO_3 data (Sites U1331, U1332, U1333 and U1334) were then generated in the Stable Isotope Ratio Mass Spectrometry Laboratory at the University of Southampton using an AutoMate automated preparation device coupled to a UIC CM5015 CO_2 coulometer. Samples weighing 1–8 mg were individually reacted in phosphoric acid, and carbonate content was calibrated using powdered Carrera marble standards of known wt% CaCO_3 measured throughout the run and at varying weights to bracket the carbonate mass ranges for the samples. A consistency standard of pure CaCO_3 and blanks were measured alongside the samples to monitor instrument performance and analytical precision, facilitate drift correction, and normalize all values to 100 wt% CaCO_3 . The limit of detection was 0.05% CaCO_3 . CaCO_3 content data for Site 1218 are from Coxall et al. (2005) and Lyle et al. (2005). Carbonate content data for Sites 1217, 1219, and 1220 were generated using the same methods as in Coxall et al. (2005).

These data were then used to calibrate the normalized median scaled (NMS) XRF core scanning datasets to provide highly resolved records of carbonate content. XRF core scanning data for Sites U1334, U1333, and 1218 are from Westerhold et al. (2014). XRF core scanning data for Sites 1219, 1220, U1331, and U1332 were generated at MARUM, University of Bremen, using the AVAATECH XRF Core Scanner III. XRF core scanning data for Site 1217 were generated at the IODP Gulf Coast Repository (GCR), using the AVAATECH Core Scanner. All data were generated at 2-cm resolution following the revised composite splice of Westerhold et al. (2012). The 1.2 cm² measurement area was defined with a 10 mm down-core slit size using optimized generator settings of 10 kV, a 0.12 mA current, and 20 s count time. Split core surfaces were leveled with a glass slide prior to application of a 4-micron-thin Ultralene film to minimize sediment desiccation and prevent down-core contamination of the XRF measurement unit. Raw data spectra were generated by a Canberra X-PIPS Detector and an Oxford Instruments 100W Neptune rhodium (Rh) X-ray tube and subsequently processed by the Canberra Eurisys iterative least square software (WIN AXIL) package. Carbonate content for the EOT interval at Site 1090 was estimated using Ca counts from XRF core scanning data of Hole 1090B cores, generated at MARUM, University of Bremen, using the AVAATECH XRF Core Scanner I, and calibrated using discrete sample CaCO_3 measurements reported by Anderson and Delaney (2005) and Diekmann et al. (2004). CaCO_3 estimates spanning Hole 1090B core gaps in the composite sequence were made using calibrated spectrophotometric data from Holes 1090D and 1090E (L*; Gersonde et al., 1999).

Bulk sediment mass accumulation rates (MARs) for the Pacific Ocean sites were calculated using estimates of dry bulk density derived from moisture-corrected gamma-ray attenuation (GRA) density data (Lyle et al., 2002; Pälike et al., 2010) and linear sedimentation rates calculated between tie points in the common astronomically tuned age model (Westerhold et al., 2014). Calcium carbonate mass accumulation rates (CaCO_3 MARs) were then calculated by multiplying MARs and the calibrated NMS XRF CaCO_3 content records. CaCO_3 MAR records were evenly sampled and smoothed using a Gaussian-weighted filter (filter width: 50 Kyr). To calculate the depth of the CCD, we used the CaCO_3 MAR gradient method of Lyle et al. (2005, 2019) whereby the depth at which CaCO_3 MAR reaches zero is estimated by dividing CaCO_3 MAR at the deepest site by the gradient of CaCO_3 MAR with water depth (Figure S2 in Supporting Information S1). Our calculations do not account for variability in export productivity or sediment focusing, however, our method provides a reasonable first order estimate of CCD depth because our data record very large changes in carbonate content over time (0–95 wt% CaCO_3) which greatly exceed the spatial variability observed in modern core-tops from the equatorial Pacific (Broecker & Peng, 1982).

3. Results and Discussion

3.1. A New Isotope Stratigraphy for the EOT in the Equatorial Pacific

Our new benthic foraminiferal stable isotope stratigraphy from Site U1334 provides a more detailed and complete record of latest Eocene climate than previously available and calls for a reappraisal of the sequence of events in the

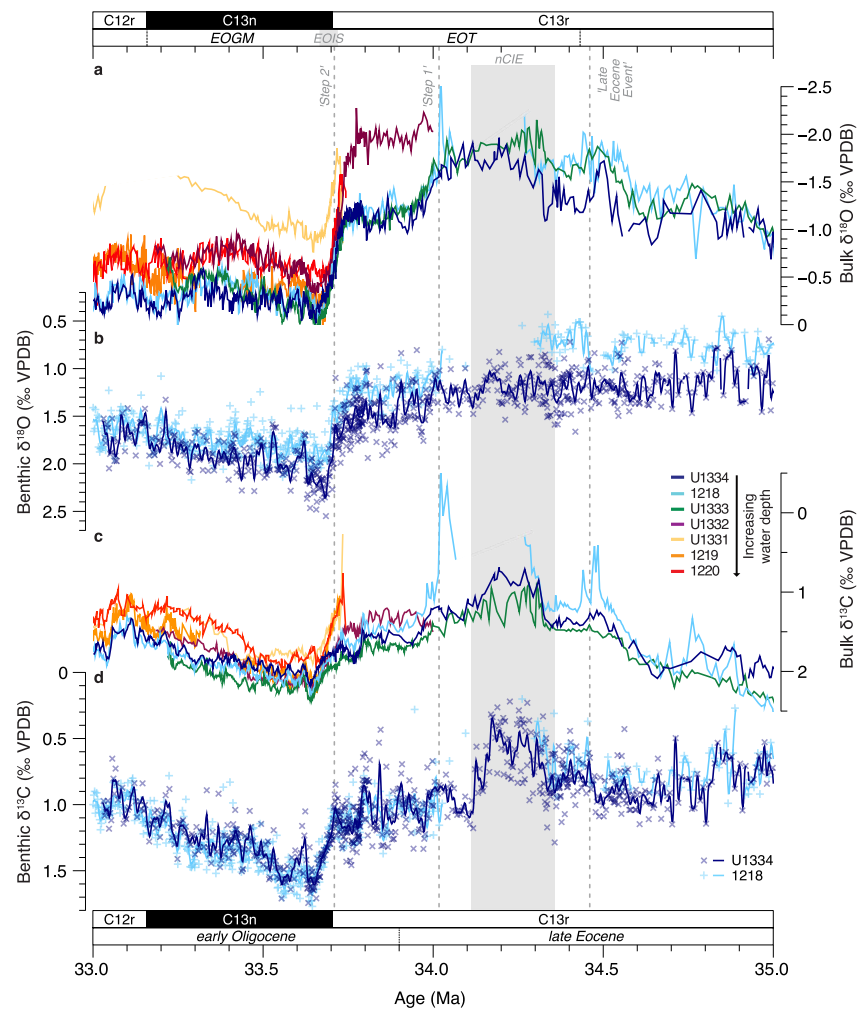


Figure 2. New stable isotope stratigraphy for the Eocene-Oligocene Transition (EOT) in the equatorial Pacific Ocean. Panels (a) and (b) show oxygen isotope series in bulk sediments (a) and benthic foraminifera (b). Panels (c) and (d) show carbon isotope series in bulk sediments (c) and benthic foraminifera (d). Bulk sediment data are from Sites U1331–U1334 and 1219–1220 (this study) and Site 1218 (Coxall et al., 2005). Data for benthic foraminifera are from Sites U1334 (dark blue, this study; *Cibicidoides grimsdalei*) and 1218 (light blue, *Cibicidoides* spp.; Coxall et al., 2005; Coxall & Wilson, 2011). Benthic foraminiferal stable isotope data are shown together with a smoothed line fit using a Gaussian-weighted filter (filter width: 20 Kyr).

run up to sustained Antarctic glaciation. First, our record shows no evidence for a late Eocene transient glaciation (Figure 2, “Late Eocene Event”) as interpreted at St. Stephen’s Quarry (Katz et al., 2008) and, tentatively, at Site 1218 (Coxall & Wilson, 2011). At Site 1218, the Late Eocene Event falls within a pronounced carbonate content minimum (Coxall et al., 2005; Coxall & Wilson, 2011). It is, therefore, possible that the transient $\delta^{18}\text{O}_b$ increase interpreted at Site 1218 is accentuated by stratigraphic condensation. Second, and most notably, the first of the two rapid increases to higher $\delta^{18}\text{O}_b$, Step 1, identified at Site 1218 (Coxall et al., 2005; Coxall & Wilson, 2011) and elsewhere (e.g., Bohaty et al., 2012; Pearson et al., 2008; Zachos et al., 1996), is not rapid or step-like in form in the stratigraphically more complete and carbonate-rich section at Site U1334 (Figure 2). Instead, our new $\delta^{18}\text{O}_b$ record increases gradually from about 1.2 to $\sim 1.7\text{‰}$ over about 300 Kyr between ~ 34.0 and ~ 33.7 Ma (Figure 2) before increasing abruptly by $\sim 0.8\text{‰}$ within ~ 40 Kyr (Step-2 or “EOIS”) to an earliest Oligocene maximum ($\sim 2.6\text{‰}$) that persisted for ~ 80 Kyr (Figure 2). Thus, our new benthic oxygen isotope record for the EOT is broadly consistent with the record from Site 1218 except for one important distinction: our new data strongly suggest that the rapid $\delta^{18}\text{O}_b$ increase in the latest Eocene (Step 1) was a distortion introduced into the Site 1218 record by stratigraphic condensation associated with the approximately 1 m-thick, ~ 300 Kyr-long, interval of non- CaCO_3 deposition (Figure 2).

Our new carbon isotope record is also highly consistent with the record from Site 1218 with one major exception (Figure 2). Our new data spanning the interval correlative to the condensed carbonate-free layer in Site 1218 reveal a pronounced transient negative carbon isotope excursion (nCIE; $\sim 0.7\text{‰}$) between ~ 34.35 and ~ 34.10 Ma (Figure 2). The late Eocene nCIE takes an asymmetric form in our record because, while the overall decrease to lower $\delta^{13}\text{C}_b$ occurs gradually (over ~ 200 Kyr), the recovery is faster (within ~ 50 Kyr) and reaches a post-excursion baseline that is $\sim 0.2\text{‰}$ higher than prior to the excursion (Figure 2). Deep-sea records from the Southern Ocean (ODP Leg 113, Site 689, and ODP Leg 119 Site 744; Diester-Haass & Zahn, 1996; Zachos et al., 1996), and South Atlantic (DSDP Leg 73, Site 522 and ODP Leg 177, Site 1090; Pusz et al., 2011; Zachos et al., 1996) and possibly the Labrador Sea (ODP Leg 105, Site 647; Coxall et al., 2018) show low $\delta^{13}\text{C}$ values in this interval and a late Eocene negative $\delta^{13}\text{C}$ excursion is also reported from a shallow marine section on the southern Australia margin (Port Willunga Beach; Haiblen et al., 2019). These observations suggest that the late Eocene nCIE event documented by our records represents a perturbation to the $\delta^{13}\text{C}$ composition of the dissolved inorganic carbon pool of the oceans globally thus making it both stratigraphically useful and interesting from a carbon cycling perspective.

3.2. Site-To-Site Correlation Along the Pacific Ocean Depth Transect

Our bulk sediment stable isotope series verify the site-to-site correlations of Westerhold et al. (2012, 2014) along the EEP transect. All of the bulk sediment stable isotope records display an EOT-diagnostic structure of abrupt increases in both $\delta^{13}\text{C}$ and $\delta^{18}\text{O}$ in the earliest Oligocene, which are closely aligned (Figure 2). Systematic offsets to lower bulk sediment $\delta^{18}\text{O}$ values are observed in records from deeper sites relative to those from the shallower sites. This bulk sediment $\delta^{18}\text{O}$ offset is most pronounced at Site U1332, at the top of C13r (~ 34.0 – ~ 33.7 Ma), where bulk sediment $\delta^{18}\text{O}$ values are $\sim 0.7\text{‰}$ lower than those of the shallow water sites (Sites U1334, 1218, and U1333; Figure 2). These bulk sediment $\delta^{18}\text{O}$ offsets are likely explained by a combination of (a) steep latitudinal gradients in surface ocean temperature and salinity, (b) coccolithophore growth rates across the EEP, which can all impact nannofossil $\delta^{18}\text{O}$ values (Hermoso, 2014), and (c) some degree of selective dissolution of taxa/size classes between shallower and deeper sites. In the early Oligocene, mean bulk sediment $\delta^{13}\text{C}$ values in records from the deepest sites are slightly lower than those from the shallower sites (Figure 2). The sign of the systematic offsets in the $\delta^{18}\text{O}$ records suggests that this feature of the $\delta^{13}\text{C}$ records is not explained by stronger recrystallization of bulk carbonate from deeper sites (Figure 2). In any case, our main focus with these bulk carbonate isotope data is chemostratigraphy and therefore the temporal change (not absolute values) documented, which is remarkably consistent among sites for both $\delta^{13}\text{C}$ and $\delta^{18}\text{O}$. Strong site-to-site consistency in bulk sediment stable isotope records is observed on a range of timescales in the this region and likely explained by the strong influence of mixed layer conditions on bulk carbonate stable isotope records making them a valuable tool for correlation (e.g., Drury et al., 2018; Reghellin et al., 2015, 2020; Shackleton & Hall, 1995). Moreover, the consistency in bulk sediment $\delta^{13}\text{C}$ and $\delta^{18}\text{O}$ among sites in our data demonstrates the stratigraphic robustness of the XRF data-based site-to-site correlations and common astronomically calibrated age model across the PEAT transect (Westerhold et al., 2012, 2014).

Comparison of our benthic stable isotope stratigraphy with the bulk sediment stable isotope series from the three sites where palaeo-water depth is shallowest and Eocene strata are carbonate-bearing (Sites U1334, 1218, and U1333), shows that the main chemostratigraphic features seen in the benthic records are also recorded by the bulk sediments (Figure 2 and Figure S3 in Supporting Information S1). There is more pronounced late Eocene variability in the bulk stable isotope records than in the benthic foraminiferal stable isotope records, especially for $\delta^{18}\text{O}$ (Figure 2 and Figure S3 in Supporting Information S1) and, while the depauperate assemblages prevent us from developing a record from planktic foraminifera, we can rule out a pervasive diagenetic control on these three bulk sediment stable isotope series because of the site-to-site consistency between records (Figure 2), shallow burial depths, and lack of correspondence between the structure of stable isotope variation and CaCO_3 content (Figures 3 and 4).

3.3. CCD Behavior at the EOT in the Equatorial Pacific Ocean

To investigate the detailed behavior of the CCD, we first consider CaCO_3 content change in the depth domain for all seven studied sites along our Pacific Ocean depth transect (Figure 3 and Figure S4 in Supporting Information S1). At all sites, upper Eocene radiolarian- and clay-rich sediments are overlain by lower Oligocene

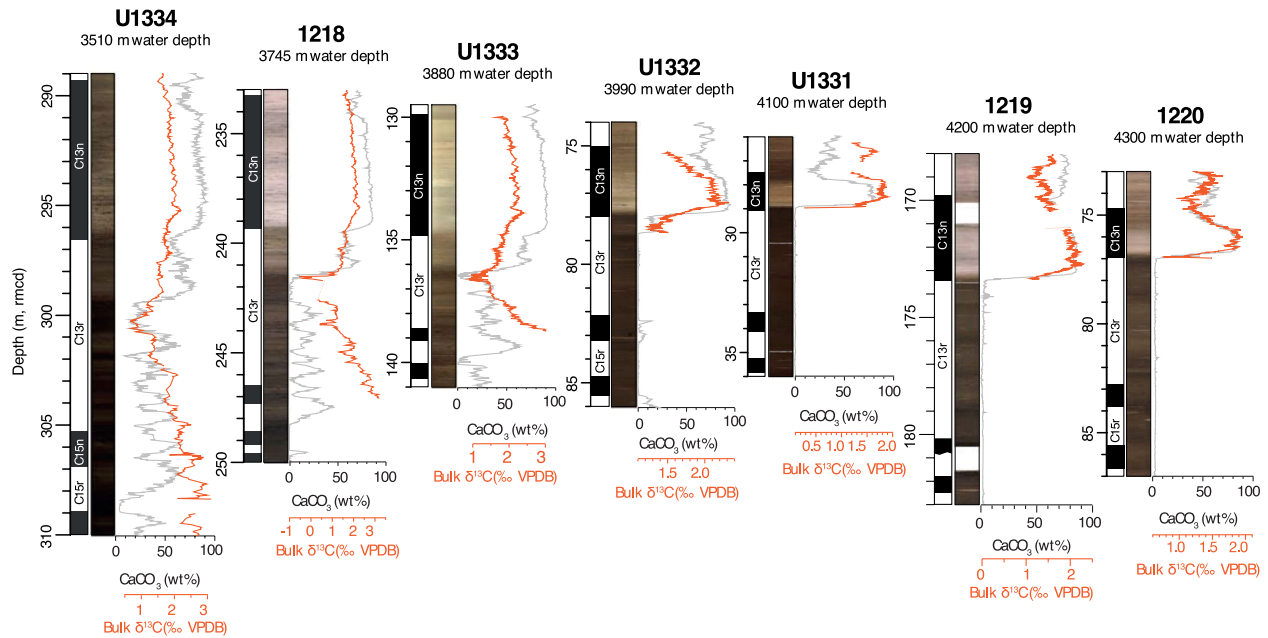


Figure 3. Composite core images, carbonate content and bulk sediment $\delta^{13}\text{C}$ records for sites along the palaeowater depth transect of sites in Eastern Equatorial Pacific showing upper Eocene to lower Oligocene strata. Records are plotted versus the revised composite core (rmcd) depths of Westerhold et al. (2014), shown in order of increasing water depth, and proportionally scaled in the depth domain. Note that the sequences become increasingly condensed with increasing water depth. Carbonate content (wt% CaCO_3) records are the result of calibrating normalized median scaled (NMS) x-ray fluorescence (XRF) core scanning datasets with discrete wt% CaCO_3 measurements. A comparison of the calibrated NMS XRF core scanning record of carbonate content and the discrete wt% CaCO_3 measurements is shown in Figure S4 in Supporting Information S1. Bulk sediment $\delta^{13}\text{C}$ records are all from this study except for Site 1218 (from Coxall et al., 2005). Site U1334 shows the same distinct stepwise downhole color change through the Eocene–Oligocene Transition as other sites in the eastern equatorial Pacific but this transition takes place within darker more clay-rich and Mn-rich nannofossil chalks than elsewhere. This is consistent with shipboard magnetic susceptibility values which are consistently higher at U1334 compared to the closest site (U1333; Pálíke et al., 2010).

calcareous oozes (Figure 3), but our data reveal four striking relationships between CaCO_3 content and water depth (Figure 3). First, at the shallow end of our transect, sediments of late Eocene age contain CaCO_3 in varying amounts (10–65 wt%) while correlative strata from our deepest sites are carbonate-free (Figure 3). Second, the calcareous oozes of the lowermost Oligocene thin markedly with increasing paleo-water depth. Magnetochron C13n is three times thicker at our shallowest site (Site U1334; 7.27 m) than at our deepest site (Site 1220; 2.27 m) (Figure 3). Third, the transition in CaCO_3 content between the underlying clay-rich sediments and overlying carbonate oozes is sharp (Figure 3). Fourth, the two-step CaCO_3 increase originally reported at Site 1218 (Coxall et al., 2005) is evident at all sites situated in water depths shallower than 4,000 m. At Site U1334, the first and second step increases in wt% CaCO_3 occur over 0.38 and 0.46 m (rmcd), respectively. In contrast, at sites situated in water depths deeper than 4,000 m, the transition from carbonate-free sediments to calcareous ooze (≥ 80 wt%) occurs in one abrupt shift over a few tens of centimeters near the base of magnetochron C13n (0.18 m, rmcd, at Site U1331; Figure 3).

In the age domain, we identify two further defining features in our CCD reconstruction for the EEP (Figures 4 and 5). First, the pronounced variations in CaCO_3 content during the latest Eocene seen at all sites situated above 4,000 m water depth are time-correlative (Figure 4). The independent stratigraphic constraints provided by our bulk sediment and benthic foraminiferal stable isotope series (Figure 2) are valuable in this regard because they provide independent confirmation of the site-to-site correlations (Westerhold et al., 2014). This CaCO_3 content variability culminates in the latest Eocene in an especially distinct interval of reduced CaCO_3 burial that lasts for ~ 300 Kyr (Figure 3). At Site 1218, this ~ 300 Kyr-long interval is represented by a condensed, ~ 1 -m thick clay-rich layer characterized by no CaCO_3 burial (Figures 3 and 4). At the top of our depth transect, at Site U1334, carbonate burial also decreases in this interval but it does not fall to zero (Figures 3 and 4). Our data, therefore, document a temporary shoaling of the CCD by at least 200 m (between $\sim 3,900$ and $\sim 3,700$ meters below sea level [mbsl]) over a ~ 300 Kyr-long interval, immediately prior to the EOT two-step CCD deepening (Figure 5). The CCD then deepens rapidly (within ~ 40 Kyr), beyond its pre-shoaling baseline by ~ 200 m to $\sim 4,000$ mbsl,

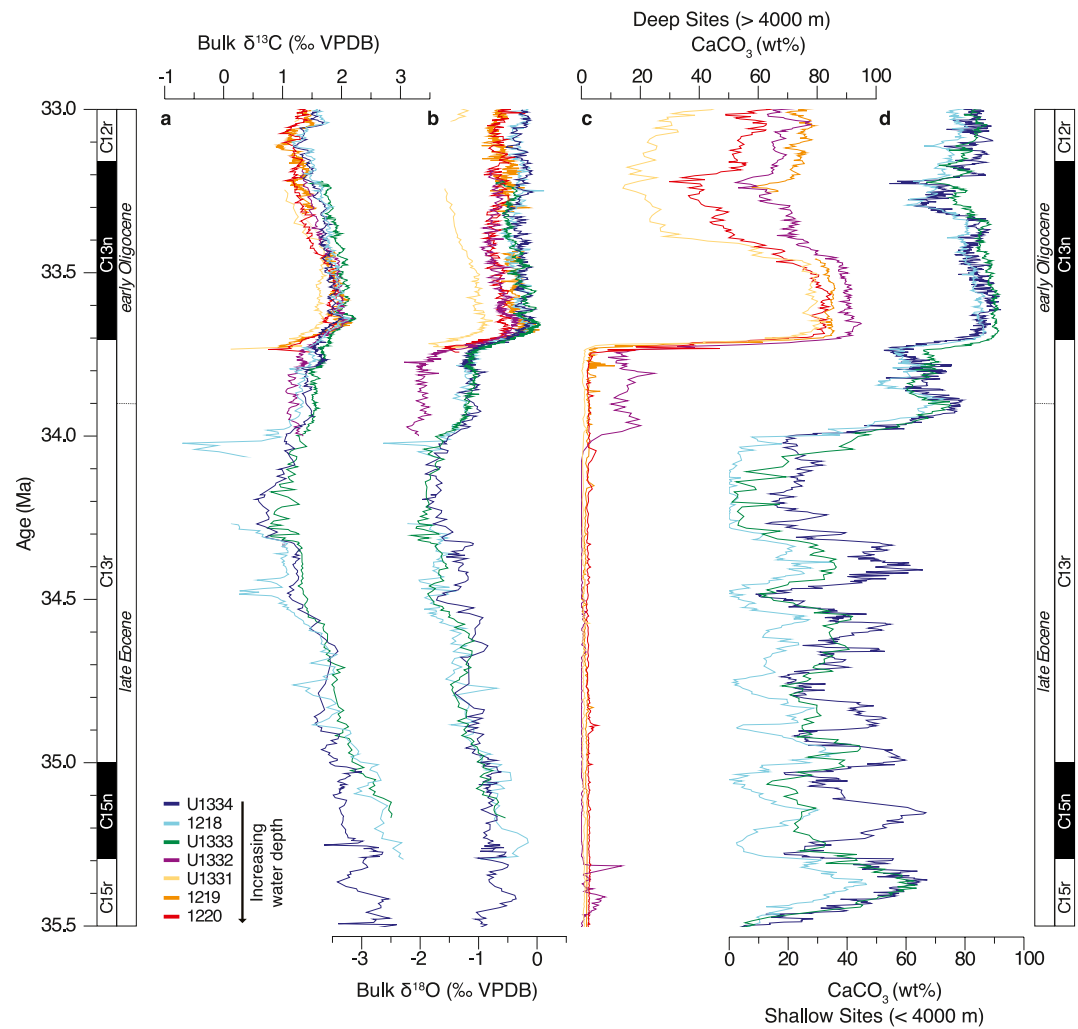


Figure 4. Bulk sediment $\delta^{13}\text{C}$ and $\delta^{18}\text{O}$ series and carbonate content records versus age for Pacific depth transect of sites spanning the late Eocene to early Oligocene. Panels (a) and (b) show bulk sediment $\delta^{13}\text{C}$ and $\delta^{18}\text{O}$ records, respectively. Note that these data independently confirm site-to-site stratigraphic correlations (see text). Panels (c) and (d) show carbonate content (wt%) records for sites $>4,000$ m (c) and $<4,000$ m (d) palaeowater-depth. Bulk sediment records are all from this study except for Site 1218 (from Coxall et al., 2005). Key lists sites from top to bottom in order of increasing water-depth (see inset in Figure 1).

and carbonate accumulates for the first time at Site U1332 (Figure 5). This is the first of the two EOT CCD deepening steps previously documented at Site 1218 by Coxall et al. (2005) and our new data show that it represents recovery from the latest Eocene CCD shoaling event (Figure 5).

The second defining feature of our CCD record in the age domain is that peak CaCO_3 content (>80 wt%; Figure 4) and accumulation rates (Figure 5) are reached synchronously at all EEP sites in the earliest Oligocene (~ 33.7 Ma; Figure S5 in Supporting Information S1), revealing that the CCD deepens rapidly well below our deepest site before rebounding to about 4,400 mbsl over an interval of about 300 Kyr (~ 33.7 – ~ 33.4 Ma; Figure 5). Thus, our data reveal a well-defined over-deepening and settling pattern. This finding strongly suggests that the transition between Cenozoic CCD regimes at the EOT occurred in response to a perturbation in oceanic carbonate fluxes that was driven by changes in deep ocean chemistry with transitory carbonate fluxes far exceeding their new steady state values.

The presence of CaCO_3 in lowermost Oligocene strata at ODP Site 1220 (Figure 4; $\sim 4,300$ m palaeo-water depth at 33.7 Ma), Deep Sea Drilling Project Site 69 (Tracey et al., 1971) ($\sim 4,500$ m palaeo-water depth at 33.7 Ma; Figure S6 in Supporting Information S1), and ODP Site 1217 ($\sim 4,400$ m palaeo-water depth at 33.7 Ma;

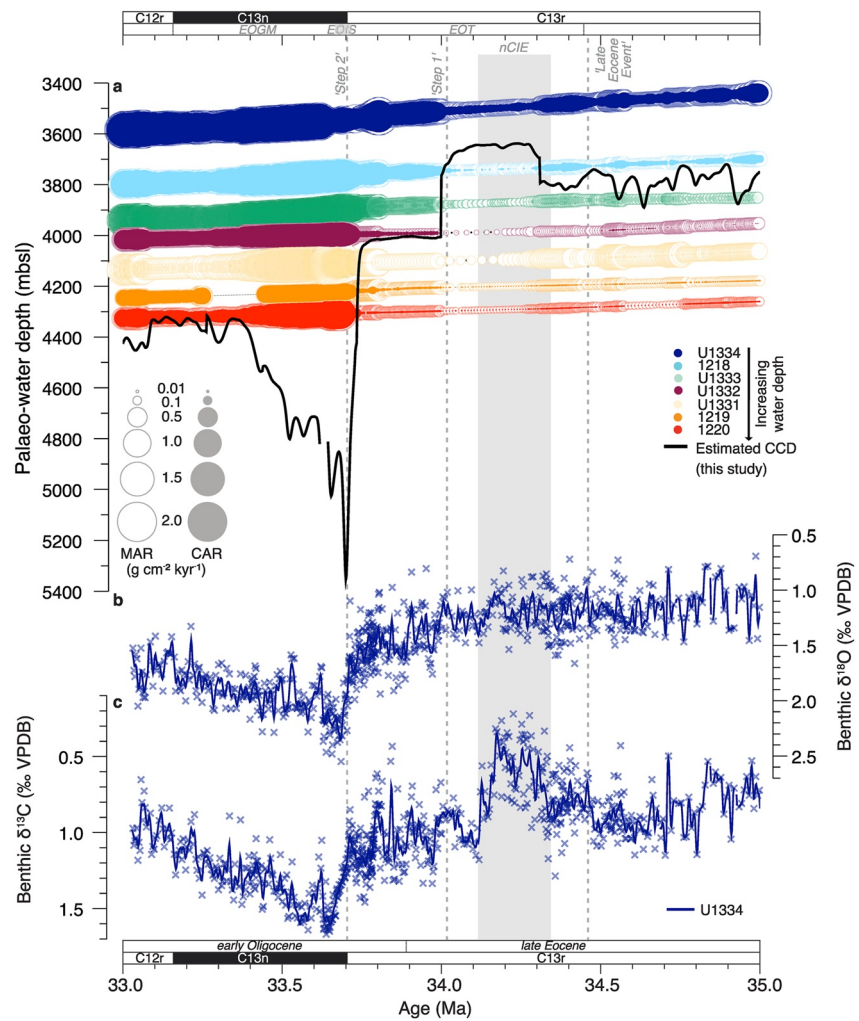


Figure 5. New high-resolution record of calcite compensation depth and benthic stable isotope stratigraphy for the Eocene Oligocene Transition in the Equatorial Pacific Ocean. (a) Carbonate accumulation rates for Sites U1331–U1334 and 1218–1220 with inferred calcite compensation depth (CCD) variability (black line). CaCO_3 MARs track the patterns recorded in wt% CaCO_3 , and changes in CaCO_3 MAR account for most of the variability observed in bulk sediment MAR. Sites 1333 and U1331 were not used in our best estimate CCD reconstruction (shown) because these two sites show slightly greater carbonate contents and CaCO_3 MARs than expected for their water depth because of the minor secondary influence of latitudinal changes in EEP export productivity (see text). (b) and (c) high resolution monospecific epifaunal (*Cibicoides grimsdalei*) $\delta^{18}\text{O}$ and $\delta^{13}\text{C}$ stratigraphy for Site U1334. Benthic foraminiferal stable isotope data are shown together with a smoothed line fit using a Gaussian-weighted filter (filter width: 20 Kyr).

Figure S7 in Supporting Information S1 which lies well north of the equatorial carbonate zone (Figure 1), indicates that, at ~ 33.7 Ma, the CCD initially deepened to at least 4.5 km in the Pacific Ocean and, by our calculation, at the peak of the EOT carbon cycle perturbation, exceeded 5 km water depth (Figure 5). This calculation is supported by observations from the modern ocean because, during the EOT over-deepening interval, carbonate contents of 80–95 wt% are reached and maintained across the entire water depth transect (Figure 4) while, in modern core-top samples from the equatorial Pacific, such high carbonate contents are only consistently found at least 500–800 m above the CCD (Broecker & Peng, 1982) (Figure 5). Thus, the CCD deepened by over 1,000 m during the second of the EOT steps alone (an over-deepening of at least 700 m) (Figure 5) and, if globally representative, would have resulted in more than a doubling of the sea floor area burying carbonate (Figure S8 in Supporting Information S1) which is comparable to that determined from a sparser dataset by Rea and Lyle (2005). Following the over-deepening event, the CCD shoaled gradually by ~ 700 m over about 300 Kyr, settling to a new steady state depth of $\sim 4,400$ m by ~ 33.4 Ma (Figure 5). The CCD settling to this shallower long-term Oligocene level will have exposed carbonate recently deposited in deeper waters to dissolution. Thus,

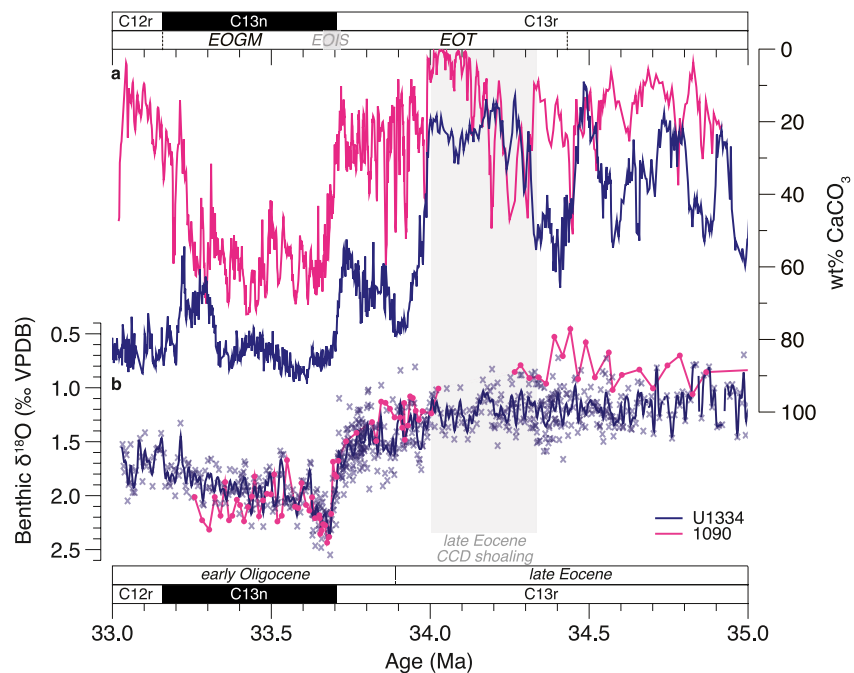


Figure 6. Comparison of carbonate content records in the Equatorial Pacific and South Atlantic oceans. (a) Carbonate content from ODP Site 1090 in the South Atlantic (pink) and IODP Site U1334 in the EEP (blue). (b) Benthic foraminiferal $\delta^{18}\text{O}$ records from Site U1334 (blue) and South Atlantic Site 1090 (pink; Pusz et al., 2011). Site U1334 benthic foraminiferal stable isotope data are shown together with a smoothed line fit using a Gaussian-weighted filter (filter width: 20 Kyr).

the full magnitude of CCD deepening is unlikely to have been preserved in the geological record even if our equatorial Pacific Ocean transect extended to abyssal levels (see Walker & Opdyke, 1995 for a fuller discussion).

3.4. CCD Behavior in the Subpolar South Atlantic Ocean

To test the extent to which the CCD record from our depth transect is representative of EOT variability outside of the equatorial Pacific Ocean, we produced a CaCO_3 content record from subantarctic South Atlantic Site 1090 (Figure 6). The relative trends in data show strong similarities between the South Atlantic and equatorial Pacific (Figure 6), with Site 1090 displaying both the latest Eocene dissolution interval and two-stage increase in wt% CaCO_3 across the EOT. Records from Sites 1053, 929, and 699 also suggest a similar overall structure of change in carbonate accumulation, suggesting this may be an Atlantic-wide feature (Borrelli et al., 2021), while mapping of the dominant sediment type indicates an increase in global carbonate sedimentation in the early Oligocene (Wade et al., 2020). These similarities between different regions/ocean basins suggest that the CCD behavior documented was primarily driven by changes in deep-water chemistry. Our data from the EEP transect suggests that the CCD lay at marginally greater depths at off-equator sites but the strong correspondence between our records from the Pacific and South Atlantic suggests that the influence of regional top-down processes (export productivity) were negligible in comparison to the processes that controlled changes in deep ocean carbonate ion concentration globally (Figures 4 and 5). CCD reconstructions from additional sites, particularly over depth transects, are needed to determine whether the earliest Oligocene over-deepening event occurred globally, but the short-term late Eocene shoaling event is clearly a prominent feature in our records from both the Pacific and Atlantic Oceans (Figure 6).

A record of the ratio of reactive phosphorous to wt% CaCO_3 at Site 1090 (Anderson & Delaney, 2005) suggests that carbonate dissolution in the subpolar South Atlantic during the latest Eocene CCD shoaling event was not driven by a reduction in export production, implying support for carbonate burial variability driven by large-scale changes in deep ocean carbonate chemistry. A minimum in carbonate content during upper magnetochron C13r is also reported for the deep equatorial Atlantic (ODP 154, Site 929; Pälike et al., 2012). Taken together, these lines of evidence suggest that the global ocean underwent a transient acidification event about 300 Kyr before the initiation of sustained large-scale Antarctic glaciation at the EOT.

3.5. Carbon Cycle Perturbation During the Late Eocene

Our records from Site U1334 show that the late Eocene transient CCD shoaling event was closely associated with a nCIE (Figure 5). The timing of the inception of these two events is similar (around 34.4 Ma) but the CCD shoaling event outlasted the nCIE by more than 100 Kyr (Figure 5 and Figure S8 in Supporting Information S1). Neither of these two changes in the carbon cycle are associated with a pronounced decrease (warming signal) in $\delta^{18}\text{O}_b$ (Figure 5). This terminal Eocene carbon cycle perturbation, therefore, differs from the hyperthermal events that occurred earlier in the Eocene, which are generally associated with a 1–2‰ nCIE, deep-sea warming (decrease in $\delta^{18}\text{O}_b$) and carbonate dissolution, and last roughly 40–100 Kyr (e.g., Sexton et al., 2011; Turner et al., 2014; Westerhold et al., 2018). Furthermore, while more records are needed to confirm the detailed form of the latest Eocene event, our data suggest that this latest Eocene carbon cycle perturbation is asymmetric—with a gradual onset, and rapid recovery phase (Figure 5). This asymmetry is opposite in form to that of the Paleocene-Eocene Thermal Maximum (PETM; ~56 Ma) where the onset phase is rapid, followed by a more gradual recovery (Röhl et al., 2007; Zachos et al., 2008).

Recovery from the latest Eocene CCD shoaling event (the first of the two EOT CCD deepening steps) is associated with a signal (increased $\delta^{18}\text{O}$ in our bulk records) suggestive of surface ocean cooling in the equatorial Pacific (Figure 4). However, the absence of evidence for a strong warming signal (in $\delta^{18}\text{O}_b$) associated with the latest Eocene carbon cycle perturbation suggests a mechanism that provokes only a minimal net increase in atmospheric CO_2 -led radiative warming. This inference is consistent with evidence for global cooling during the early phases of the EOT (e.g., Bohaty et al., 2012; Houben et al., 2019; Katz et al., 2008; Liu et al., 2009). In principle, a decreased carbonate weathering flux into the global ocean can trigger CCD shoaling with no CO_2 -led warming and produce a nCIE through $\delta^{13}\text{C}$ fractionation between the carbonate weathering and burial flux. This would, however, require carbonate and silicate weathering fluxes to become decoupled (Armstrong McKay et al., 2016; Merico et al., 2008). Another possibility is that the nCIE was driven by the gradual introduction into the ocean of carbon from a reservoir extremely enriched in ^{12}C , presumably from marine or terrestrial sediments. One possible source could be the high nutrient, Arctic-imprinted, northern component water mass characterized by Coxall et al. (2018). Southward export of this water mass has been suggested to explain an interval of low $\delta^{13}\text{C}_b$ in the North Atlantic Ocean that is broadly temporally consistent with the nCIE observed in the EEP (Coxall et al., 2018). A third possibility is that increases in global volcanic carbon emissions play a role in driving the nCIE. A slow increase followed by a relatively rapid relaxation of global volcanic carbon emissions (an isotopically depleted source) could explain the latest Eocene $\delta^{13}\text{C}_b$ increase and cooling (increasing $\delta^{18}\text{O}$) that follows the recovery from the nCIE. Further work, including modeling experiments, is needed to understand the origin of this late Eocene carbon cycle perturbation, but our data strongly suggest this event is a defining feature of the early phase of the EOT and that recovery of the carbon cycle from this perturbation led directly to the first of the two EOT CCD deepening steps originally documented at Site 1218 (Coxall et al., 2005).

3.6. CCD Deepening and the Onset of Antarctic Glaciation

Based on the records from Site 1218, Coxall et al. (2005) inferred a lockstep relationship between the two EOT CCD deepening steps and deterioration of high latitude climate as registered by $\delta^{18}\text{O}_b$. Our new data suggest that the coupling between basification of the deep ocean and cooling of the high latitudes develops later during the EOT than previously inferred. In the records from Site U1334, the first EOT CCD deepening step is associated with modest cyclicity (not a step-increase) in $\delta^{18}\text{O}_b$ (Figure 5 and Figure S9 in Supporting Information S1). Furthermore, for the second EOT CCD deepening step, although the peaks in carbonate content and $\delta^{18}\text{O}_b$ are in phase (Coxall & Wilson, 2011), close inspection of the timing of the onset of the increases in $\delta^{18}\text{O}_b$ and carbonate content in the records from Sites U1334 and 1218 suggests that the onset of the increase in carbonate content may lead the onset of the increase in $\delta^{18}\text{O}_b$ by roughly 0.25 and 0.35 m (rmcd), respectively (corresponding to roughly 20 and 30 Kyr, respectively; Figure S10 in Supporting Information S1). This relationship cannot be explained by the reworking up-section of finer sedimentary components (see the related PETM discussion in Hupp & Kelly, 2020), but it may perhaps be explained by differential sediment mixing (bioturbation). The presence of a similar relationship at Site 1090 (Figures S11 and S12 in Supporting Information S1), however, suggests that the observed phase relationship at the equatorial Pacific sites represents a true lead-lag relationship between the onset of EOT CCD deepening in the EEP and the inception of major Antarctic glaciation as recorded by $\delta^{18}\text{O}_b$. Further work is needed to understand the implications of this result. One possibility is that the validity of the shelf-basin

fractionation hypothesis is called into question, at least as the initial trigger mechanism for CCD deepening. However, our data may simply reflect different sensitivities of $\delta^{18}\text{O}_b$ and CaCO_3 accumulation to ice growth and sea level fall during the earliest stages of Antarctic ice growth. Either way, our records show that, at least in the EEP, the CCD over-deepened markedly (down to ~ 5 km) between ~ 33.7 and ~ 33.4 Ma before settling, implying that abrupt increases occurred in both deep ocean carbonate ion concentration and sea floor carbonate burial to values greatly exceeding their new steady state ones (Figure 5). The (over)deepening and settling pattern that we document is highly consistent with the shelf-basin fractionation hypothesis, which comprises two processes resulting from glacioeustatic sea level fall: (a) a sustained shift in the locus of global carbonate burial from the shelves to the deep ocean and (b) a short-term spike in carbonate ion flux to the global ocean driven by exposure of fresh, readily weathered carbonate deposits on land (Armstrong McKay et al., 2016; Merico et al., 2008). CCD deepening occurs until the carbonate burial output flux from the ocean to pelagic oozes is large enough to restore balance with global carbonate inputs to the ocean.

4. Conclusions

Highly resolved carbonate accumulation and stable isotope records spanning a depth transect in the EEP provide new constraints on the EOT transition between two Cenozoic CCD regimes from a highly variable shallow CCD regime pre-EOT to the comparatively well-buffered regime of the post-EOT icehouse world. We detail three main new features of the CCD record: (a) a latest Eocene global carbon cycle perturbation defined by a CCD shoaling event and a prominent negative carbon isotope excursion leading directly into the two step EOT CCD deepening; (b) a distinctive over-deepening (down to ~ 5 km in the equatorial Pacific Ocean) and settling pattern in the earliest Oligocene diagnostic of distinctly non-steady state change from the early Cenozoic to later Cenozoic CCD regimes; (c) evidence from the South Atlantic that these CCD changes were not merely regional and therefore likely driven by changes in global deep ocean chemistry. Recovery from the latest Eocene carbon cycle perturbation drove the first EOT CCD deepening step while the second over-deepening step was closely coupled to the inception of sustained large-scale Antarctic glaciation. Thus, we propose that the carbon cycle was perturbed during the EOT before the inception of Antarctic glaciation yet, once glaciation was initiated, rapid changes in global seawater chemistry triggered a transient increase in carbonate burial flux in the deep ocean far exceeding the new steady state values. This finding is consistent with a short-term spike in carbonate ion flux to the global ocean driven by glacioeustatic sea level fall and exposure of fresh, readily weathered carbonate deposits on land as modeled by Armstrong McKay et al. (2016) and Merico et al. (2008).

Acknowledgments

This work was supported by Natural Environment Research Council (NERC) Grants NE/I006168/1 (PAW), NE/K008390/1 (PAW), NE/K007211/1 (PAW), and NE/F003641/1 (HP, PAW and KME), a Royal Society Wolfson Merit Award to PAW, and a NERC SPITFIRE Doctoral Training Program Studentship (NE/L002531/1) awarded to VET and supervised by PAW and SMB. UR and TW were funded by the Deutsche Forschungsgemeinschaft (DFG, German Research Foundation)—Project number 179386126. The authors thank Megan Wilding, Bastian Hambach, Mike Hall, and Cristina Sghibartz for laboratory assistance, Phil Rumford, and colleagues at the IODP Gulf Coast Core Repository, for assistance with sampling, and David Armstrong McKay and Toby Tyrrell for stimulating discussions. We thank the Editor and Reviewers for their constructive and thorough reviews which improved this manuscript. For the purpose of open access, the author has applied a CC BY public copyright license to any Author Accepted Manuscript version arising from this submission.

Data Availability Statement

This research used samples and data provided by the International Ocean Discovery Program (IODP). All data are available on Pangaea at Taylor et al. (2023).

References

- Anderson, L. D., & Delaney, M. L. (2005). Middle Eocene to early Oligocene paleoceanography from Agulhas Ridge, Southern Ocean (Ocean Drilling Program Leg 177, Site 1090). *Paleoceanography*, 20(1), 1–13. <https://doi.org/10.1029/2004PA001043>
- Armstrong McKay, D. I., Tyrrell, T., & Wilson, P. A. (2016). Global carbon cycle perturbation across the Eocene-Oligocene climate transition. *Paleoceanography*, 31(2), 311–329. <https://doi.org/10.1002/2015PA002818>
- Berger, W. H., & Winterer, E. L. (1975). Plate stratigraphy and the fluctuating carbonate line. In J. D. Milliman, K. J. Hsu, & H. C. Jenkyns (Eds.), *Pelagic sediments; on land and under the sea* (pp. 11–48). Blackwell Publishing Ltd. <https://doi.org/10.2475/ajs.276.5.670>
- Bohaty, S. M., Zachos, J. C., & Delaney, M. L. (2012). Foraminiferal Mg/Ca evidence for Southern Ocean cooling across the Eocene-Oligocene transition. *Earth and Planetary Science Letters*, 317–318, 251–261. <https://doi.org/10.1016/j.epsl.2011.11.037>
- Borrelli, C., Katz, M. E., & Toggweiler, J. R. (2021). Middle to Late Eocene changes of the ocean carbonate cycle. *Paleoceanography and Paleoclimatology*, 36(12), e2020PA004168. <https://doi.org/10.1029/2020PA004168>
- Broecker, W. S., & Peng, T.-H. (1982). *Tracers in the sea*. Lamont-Doherty Geological Observatory.
- Broecker, W. S., & Peng, T. H. (1987). The role of CaCO_3 compensation in the glacial to interglacial atmospheric CO_2 change. *Global Biogeochemical Cycles*, 1, 15–29. <https://doi.org/10.1029/gb0011001p00015>
- Channell, J. E. T., Galeotti, S., Martin, E. E., Billups, K., Scher, H. D., & Stoner, J. S. (2003). Eocene to Miocene magnetostratigraphy, biostratigraphy, and chemostratigraphy at ODP Site 1090 (sub-Antarctic South Atlantic). *Bulletin of the Geological Society of America*, 115(5), 607–623. [https://doi.org/10.1130/0016-7606\(2003\)115<0607:ETMMA>2.0.CO;2](https://doi.org/10.1130/0016-7606(2003)115<0607:ETMMA>2.0.CO;2)
- Coxall, H. K., Huck, C. E., Huber, M., Lear, C. H., Legarda-Lisarrri, A., O'Regan, M., et al. (2018). Export of nutrient rich Northern Component Water preceded early Oligocene Antarctic glaciation. *Nature Geoscience*, 11(3), 190–196. <https://doi.org/10.1038/s41561-018-0069-9>
- Coxall, H. K., & Wilson, P. A. (2011). Early Oligocene glaciation and productivity in the eastern equatorial Pacific: Insights into global carbon cycling. *Paleoceanography*, 26(2), 1–18. <https://doi.org/10.1029/2010PA002021>

- Coxall, H. K., Wilson, P. A., Pälike, H., Lear, C. H., & Backman, J. (2005). Rapid stepwise onset of Antarctic glaciation and deeper calcite compensation in the Pacific Ocean. *Nature*, *433*(7021), 53–57. <https://doi.org/10.1038/nature03135>
- Dalai, T. K., Ravizza, G. E., & Peucker-Ehrenbrink, B. (2006). The Late Eocene 1870s/1880s excursion: Chemostratigraphy, cosmic dust flux and the Early Oligocene glaciation. *Earth and Planetary Science Letters*, *241*(3–4), 477–492. <https://doi.org/10.1016/j.epsl.2005.11.035>
- DeConto, R. M., & Pollard, D. (2003). Rapid Cenozoic glaciation of Antarctica induced by declining atmospheric CO₂. *Nature*, *421*(6920), 245–249. <https://doi.org/10.1038/nature01290>
- Diekmann, B., Kuhn, G., Gersonde, R., & Mackensen, A. (2004). Middle Eocene to early Miocene environmental changes in the sub-Antarctic Southern Ocean: Evidence from biogenic and terrigenous depositional patterns at ODP Site 1090. *Global and Planetary Change*, *40*(3–4), 295–313. <https://doi.org/10.1016/j.gloplacha.2003.09.001>
- Diester-Haass, L., & Zahn, R. (1996). Eocene-Oligocene transition in the Southern Ocean: History of water mass circulation and biological productivity. *Geology*, *24*(2), 163–166. [https://doi.org/10.1130/0091-7613\(1996\)024<0163:EOTITS>2.3.CO;2](https://doi.org/10.1130/0091-7613(1996)024<0163:EOTITS>2.3.CO;2)
- Drury, A. J., Lee, G. P., Gray, W. R., Lyle, M., Westerhold, T., Shevenell, A. E., & John, C. M. (2018). Deciphering the state of the late Miocene to early Pliocene equatorial Pacific. *Paleoceanography and Paleoclimatology*, *33*(3), 246–263. <https://doi.org/10.1002/2017PA003245>
- Dutkiewicz, A., Müller, R. D., Cannon, J., Vaughan, S., & Zhirovic, S. (2018). Sequestration and subduction of deep-sea carbonate in the global ocean since the Early Cretaceous. *Geology*, *47*(1), 91–94. <https://doi.org/10.1130/g45424.1>
- Edgar, K. M., Pälike, H., & Wilson, P. A. (2013). Testing the impact of diagenesis on the $\delta^{18}O$ and $\delta^{13}C$ of benthic foraminiferal calcite from a sediment burial depth transect in the equatorial Pacific. *Paleoceanography*, *28*(3), 468–480. <https://doi.org/10.1002/palo.20045>
- Ehrmann, W. U., & Mackensen, A. (1992). Sedimentological evidence for the formation of an East Antarctic ice sheet in Eocene/Oligocene time. *Palaeogeography, Palaeoclimatology, Palaeoecology*, *93*(1–2), 85–112. [https://doi.org/10.1016/0031-0182\(92\)90185-8](https://doi.org/10.1016/0031-0182(92)90185-8)
- Gersonde, R., Hodell, D. A., Blum, P., & Party, S. S. (1999). Site 1090. Initial Reports, 177. In *Proceedings of the Ocean Drilling Program*. <https://doi.org/10.2973/odp.proc.ir.177.105.1999>
- Haiblen, A. M., Opdyke, B. N., Roberts, A. P., Heslop, D., & Wilson, P. A. (2019). Midlatitude southern hemisphere temperature change at the end of the Eocene greenhouse shortly before dawn of the Oligocene icehouse. *Paleoceanography and Paleoclimatology*, *34*(12), 1995–2004. <https://doi.org/10.1029/2019PA003679>
- Hambrey, M. J., Ehrmann, W. U., & Larsen, B. (1991). Cenozoic glacial record of the Prydz Bay continental shelf, East Antarctica. In *Proc., scientific results, ODP, Leg 119, Kerguelen Plateau-Prydz Bay, September* (pp. 77–132). <https://doi.org/10.2973/odp.proc.sr.119.200.1991>
- Hermoso, M. (2014). Coccolith-derived isotopic proxies in palaeoceanography: Where geologists need biologists. *Cryptogamie Algologie*, *35*(4), 323–351. <https://doi.org/10.7872/crya.v35.iss4.2014.323>
- Houben, A. J. P., Bijl, P. K., Sluijs, A., Schouten, S., & Brinkhuis, H. (2019). Late Eocene southern ocean cooling and invigoration of circulation preconditioned Antarctica for full-scale glaciation. *Geochemistry, Geophysics, Geosystems*, *20*(5), 2214–2234. <https://doi.org/10.1029/2019GC008182>
- Hupp, B., & Kelly, D. C. (2020). Delays, discrepancies, and distortions: Size-dependent sediment mixing and the deep-sea record of the Paleocene-Eocene thermal maximum from ODP Site 690 (Weddell Sea). *Paleoceanography and Paleoclimatology*, *35*(11), 1–19. <https://doi.org/10.1029/2020PA004018>
- Hutchinson, D. K., Coxall, H. K., Lunt, D. J., Steinthorsdottir, M., De Boer, A. M., Baatsen, M., et al. (2021). The Eocene-Oligocene transition: A review of marine and terrestrial proxy data, models and model-data comparisons. *Climate of the Past*, *17*(1), 269–315. <https://doi.org/10.5194/cp-17-269-2021>
- Katz, M. E., Miller, K. G., Wright, J. D., Wade, B. S., Browning, J. V., Cramer, B. S., & Rosenthal, Y. (2008). Stepwise transition from the Eocene greenhouse to the Oligocene icehouse. *Nature Geoscience*, *1*(5), 329–334. <https://doi.org/10.1038/ngeo179>
- Koppers, A. A. P., Morgan, J. P., Morgan, J. W., & Staudigel, H. (2001). Testing the fixed hotspot hypothesis using 40Ar/39Ar age progressions along seamount trails. *Earth and Planetary Science Letters*, *185*(3–4), 237–252. [https://doi.org/10.1016/S0012-821X\(00\)00387-3](https://doi.org/10.1016/S0012-821X(00)00387-3)
- Lear, C. H., Bailey, T. R., Pearson, P. N., Coxall, H. K., & Rosenthal, Y. (2008). Cooling and ice growth across the Eocene-Oligocene transition. *Geology*, *36*(3), 251–254. <https://doi.org/10.1130/G24584A.1>
- Lear, C. H., Mawbey, E. M., & Rosenthal, Y. (2010). Cenozoic benthic foraminiferal Mg/Ca and Li/Ca records: Toward unlocking temperatures and saturation states. *Paleoceanography*, *25*(4), 1–11. <https://doi.org/10.1029/2009PA001880>
- Lear, C. H., Rosenthal, Y., Coxall, H. K., & Wilson, P. A. (2004). Late Eocene to early Miocene ice sheet dynamics and the global carbon cycle. *Paleoceanography*, *19*(4), 1–11. <https://doi.org/10.1029/2004PA001039>
- Liu, Z., Pagani, M., Zinniker, D., Deconto, R., Huber, M., Brinkhuis, H., et al. (2009). Global cooling during the Eocene-Oligocene climate transition. *Science*, *323*(February), 1187–1190. <https://doi.org/10.1126/science.1166368>
- Liu, Z., Tuo, S., Zhao, Q., Cheng, X., & Huang, W. (2004). Deep-water earliest Oligocene glacial maximum (EOGM) in South Atlantic. *Chinese Science Bulletin*, *49*(20), 2190–2197. <https://doi.org/10.1360/04wd0228>
- Lyle, M., Joy Drury, A., Tian, J., Wilkens, R., & Westerhold, T. (2019). Late Miocene to Holocene high-resolution eastern equatorial Pacific carbonate records: Stratigraphy linked by dissolution and paleoproductivity. *Climate of the Past*, *15*(5), 1715–1739. <https://doi.org/10.5194/cp-15-1715-2019>
- Lyle, M., Lyle, A. O., Backman, J., & Tripati, A. (2005). Biogenic sedimentation in the Eocene equatorial Pacific - The stuttering Greenhouse and Eocene carbonate compensation depth. In *Proceedings of the Ocean Drilling Program* (Vol. 199, pp. 1–35).
- Lyle, M., Wilson, P. A., Janecek, T. R., Backman, J., Busch, W. H., Coxall, H. K., et al. (2002). *Proc. ODP, Init. Repts.*, 199. Ocean Drilling Program. <https://doi.org/10.2973/odp.proc.ir.199.2002>
- Merico, A., Tyrrell, T., & Wilson, P. A. (2008). Eocene/Oligocene ocean de-acidification linked to Antarctic glaciation by sea-level fall. *Nature*, *452*(7190), 979–982. <https://doi.org/10.1038/nature06853>
- Miller, K. G., Browning, J. V., Aubry, M. P., Wade, B. S., Katz, M. E., Kulpecz, A. A., & Wright, J. D. (2008). Eocene-Oligocene global climate and sea-level change changes: St. Stephens Quarry, Alabama. *Geological Society of America Bulletin*, *120*(1–2), 34–53. <https://doi.org/10.1130/B26105.1>
- Müller, R. D., Mather, B., Dutkiewicz, A., Keller, T., Merdith, A., Gonzalez, C. M., et al. (2022). Evolution of Earth's tectonic carbon conveyor belt. *Nature*, *605*(7911), 629–639. <https://doi.org/10.1038/s41586-022-04420-x>
- Opdyke, B. N., & Wilkinson, B. H. (1988). Surface area control of shallow cratonic to deep marine carbonate accumulation. *Paleoceanography*, *3*(6), 685–703. <https://doi.org/10.1029/pa003i006p0685>
- Pälike, H., Lyle, M. W., Nishi, H., Raffi, I., Ridgwell, A., Gamage, K., et al. (2012). A Cenozoic record of the equatorial Pacific carbonate compensation depth. *Nature*, *488*(7413), 609–614. <https://doi.org/10.1038/nature11360>
- Pälike, H., Nishi, H., Lyle, M., Raffi, I., Gamage, K., & Klaus, A., & the Expedition 320/321 Scientists. (2010). *Proc. IODP, 320/321*. Integrated Ocean Drilling Program Management International, Inc. <https://doi.org/10.2204/iodp.sd.9.01.2010>

- Pearson, P. N., McMillan, I. K., Wade, B. S., Jones, T. D., Coxall, H. K., Bown, P. R., & Lear, C. H. (2008). Extinction and environmental change across the Eocene-Oligocene boundary in Tanzania. *Geology*, *36*(2), 179–182. <https://doi.org/10.1130/G24308A.1>
- Pusz, A. E., Thunell, R. C., & Miller, K. G. (2011). Deep water temperature, carbonate ion, and ice volume changes across the Eocene-Oligocene climate transition. *Paleoceanography*, *26*(2), 1–15. <https://doi.org/10.1029/2010PA001950>
- Rea, D. K., & Lyle, M. W. (2005). Paleogene calcite compensation depth in the eastern subtropical Pacific: Answers and questions. *Paleoceanography*, *20*(1), 1–19. <https://doi.org/10.1029/2004PA001064>
- Reghellin, D., Coxall, H. K., Dickens, G. R., & Backman, J. (2015). Carbon and oxygen isotopes of bulk carbonate in sediment deposited beneath the eastern equatorial Pacific over the last 8 million years. *Paleoceanography*, *30*(10), 1261–1286. <https://doi.org/10.1002/2015PA002825>
- Reghellin, D., Dickens, G. R., Coxall, H. K., & Backman, J. (2020). Understanding bulk sediment stable isotope records in the eastern equatorial Pacific, from seven million years ago to present day. *Paleoceanography and Paleoclimatology*, *35*(2), e2019PA003586. <https://doi.org/10.1029/2019PA003586>
- Ridgwell, A., & Zeebe, R. (2005). The role of the global carbonate cycle in the regulation and evolution of the Earth system. *Earth and Planetary Science Letters*, *234*(3–4), 299–315. <https://doi.org/10.1016/j.epsl.2005.03.006>
- Röhl, U., Westerhold, T., Bralower, T. J., & Zachos, J. C. (2007). On the duration of the Paleocene-Eocene thermal maximum (PETM). *Geochemistry, Geophysics, Geosystems*, *8*(12), Q12002. <https://doi.org/10.1029/2007GC001784>
- Scher, H. D., Bohaty, S. M., Zachos, J. C., & Delaney, M. L. (2011). Two-stepping into the icehouse: East Antarctic weathering during progressive ice-sheet expansion at the Eocene-Oligocene transition. *Geology*, *39*(4), 383–386. <https://doi.org/10.1130/G31726.1>
- Sexton, P. F., Norris, R. D., Wilson, P. A., Pälike, H., Westerhold, T., Röhl, U., et al. (2011). Eocene global warming events driven by ventilation of oceanic dissolved organic carbon. *Nature*, *471*(7338), 349–353. <https://doi.org/10.1038/nature09826>
- Shackleton, N. J., & Hall, M. A. (1995). Stable isotope records in bulk sediments (Leg 138). In N. G. Piasias, L. A. Mayer, T. R. Janacek, A. Palmer Julson, & T. H. vanAndel (Eds.), *Proceedings of the Ocean Drilling Program, scientific results* (Vol. 138, pp. 797–805).
- Taylor, V. E., Westerhold, T., Bohaty, S. M., Backman, J., Dunkley Jones, T., Egan, K., et al. (2023). Benthic foraminiferal and bulk sediment stable isotope records, and carbonate content records from the eastern equatorial Pacific, and a reconstruction of the calcite compensation depth, across the EO [Dataset]. PANGAEA. <https://doi.org/10.1594/PANGAEA.956848>
- Tracey, J. I., Sutton, G. H., Nesteroff, W. D., Galehouse, J., von der Borch, C. C., Moore, T. C., et al. (1971). Site 70. In J. I. Tracey Jr., et al. (Eds.), *Initial reports of the deep sea drilling project* (Vol. VIII, pp. 135–284). U.S. Government Printing Office. <https://doi.org/10.2973/dsdp.proc.8.105.1971>
- Turner, S. K., Sexton, P. F., Charles, C. D., & Norris, R. D. (2014). Persistence of carbon release events through the peak of early Eocene global warmth. *Nature Geoscience*, *7*(10), 748–751. <https://doi.org/10.1038/NNGEO2240>
- van Andel, T. H. (1975). Distribution of calcareous sediments. *Earth and Planetary Science Letters*, *26*(2), 187–194. [https://doi.org/10.1016/0012-821x\(75\)90086-2](https://doi.org/10.1016/0012-821x(75)90086-2)
- van Andel, T. H., Heath, G. R., & Moore, T. C., Jr. (1975). Cenozoic history and paleoceanography of the central equatorial Pacific Ocean: A regional synthesis of Deep Sea Drilling Project data. *Geological Society of America*, *143*, 1–134.
- Wade, B. S., Houben, A. J. P., Quaijtaal, W., Schouten, S., Rosenthal, Y., Miller, K. G., et al. (2012). Multiproxy record of abrupt sea-surface cooling across the Eocene-Oligocene transition in the Gulf of Mexico. *Geology*, *40*(2), 159–162. <https://doi.org/10.1130/G32577.1>
- Wade, B. S., O'Neill, J. F., Phujareanchaiwon, C., Ali, I., Lyle, M., & Witkowski, J. (2020). Evolution of deep-sea sediments across the Paleocene-Eocene and Eocene-Oligocene boundaries. *Earth-Science Reviews*, *211*, 103403. <https://doi.org/10.1016/j.earscirev.2020.103403>
- Walker, J. C. G., & Opdyke, B. C. (1995). Influence of variable rates of neritic carbonate deposition on atmospheric carbon dioxide and pelagic sediments. *Paleoceanography*, *10*(3), 415–447. <https://doi.org/10.1029/94pa02963>
- Westerhold, T., Röhl, U., Donner, B., & Zachos, J. C. (2018). Global extent of early Eocene hyperthermal events: A new Pacific benthic foraminiferal isotope record from Shatsky Rise (ODP Site 1209). *Paleoceanography and Paleoclimatology*, *33*(6), 626–642. <https://doi.org/10.1029/2017PA003306>
- Westerhold, T., Röhl, U., Pälike, H., Wilkens, R., Wilson, P. A., & Acton, G. (2014). Orbitally tuned timescale and astronomical forcing in the middle Eocene to early Oligocene. *Climate of the Past*, *10*(3), 955–973. <https://doi.org/10.5194/cp-10-955-2014>
- Westerhold, T., Röhl, U., Wilkens, R., Pälike, H., Lyle, M., Jones, T. D., et al. (2012). Revised composite depth scales and integration of IODP Sites U1331-U1334 and ODP Sites 1218–1220. 320. <https://doi.org/10.2204/iodp.proc.320321.201.2012>
- Zachos, J. C., Breza, J. R., & Wise, S. W. (1992). Early Oligocene ice-sheet expansion on Antarctica: Stable isotope and sedimentological evidence from Kerguelen Plateau, southern Indian Ocean. *Geology*, *20*(6), 569–573. [https://doi.org/10.1130/0091-7613\(1992\)020<0569:EOISEO>2.3.CO;2](https://doi.org/10.1130/0091-7613(1992)020<0569:EOISEO>2.3.CO;2)
- Zachos, J. C., Dickens, G. R., & Zeebe, R. E. (2008). An early Cenozoic perspective on greenhouse warming and carbon-cycle dynamics. *Nature*, *451*(7176), 279–283. <https://doi.org/10.1038/nature06588>
- Zachos, J. C., Quinn, T. M., & Salamy, K. A. (1996). High-resolution (104 years) deep-sea foraminiferal stable isotope records of the Eocene-Oligocene climate transition. *Paleoceanography*, *11*(3), 251–266. <https://doi.org/10.1029/96PA00571>

References From the Supporting Information

- Paillard, D., Labeyrie, L., & Yiou, P. (1996). Macintosh program performs time-series analysis. *Eos, Transactions American Geophysical Union*, *77*(39), 379. <https://doi.org/10.1029/96eo00259>